JOURNAL OF GEOPHYSICAL RESEARCH, VOL. 103, NO. A9, PAGES 20,669–20,684, SEPTEMBER 1, 1998

Ionospheric storm simulations driven by magnetospheric MHD and by empirical models with data comparisons

J. J. Sojka,[1] R. W. Schunk,[1] M. D. Bowline,[1] J. Chen,[2] S. Slinker[2], J. Fedder,[3] and P. J. Sultan[4]

Abstract. The results of two ionospheric simulations are compared with each other and with ionospheric observations of the southern hemisphere for the magnetic cloud passage event of January 14, 1988. For most of the event one simulation agrees with observations, while the other does not. Electric fields and electron precipitation patterns generated by a magnetospheric MHD model are used as inputs to a physical model of the ionosphere in the successful simulation, while empirical electric fields and electron precipitation are used as the inputs for the second simulation. In spite of ionospheric summer conditions a large and deep polar hole is developed. This is seen in the in situ plasma observations made by the DMSP-F8 satellite. The hole is surprisingly present during both northward and southward IMF conditions. It is deepest for the storm phase of the southward IMF period. A well-defined tongue of ionization is formed during this period. These features have been reproduced by the TDIM-MHD simulation and to a lesser extent by the TDIM-empirical simulation. However, the model simulations have not been able to generate a storm enhanced density where one was observed by DMSP-F8 during the initial phase of the storm. The differences between the two *F* region ionospheric simulations are attributed to differences in the magnetospheric electric fields and precipitation patterns used as inputs. This study provides a unique first simulation of the ionosphere's response to self-consistent electric field and auroral precipitation patterns over a 24-hour period that leads into a major geomagnetic storm.

1. Introduction

An interplanetary magnetic cloud took 30-hours to pass the Earth's magnetosphere beginning at about 0000 UT on January 14, 1988. This cloud event is unique in that extensive observations in the interplanetary field and in the magnetosphere-ionosphere were made and hence enabled a reconstruction of the magnetosphere's responses to the IMF changes associated with the cloud passage. During the first 16 hours the IMF B_z was northward; for the final 18 hours the IMF was southward. A magnetic storm event was associated with the later period, which was also punctuated by numerous magnetic substorms. Because the IMF B_y and B_z components varied quite systematically during the 30-hour passage, this event is ideal for studies in which the magnetospheric electric field depends critically on both the B_y and B_z components. A number of such studies have been carried out not only to predict how the magnetospheric electric field varies as a function of both B_y and B_z but also to validate these with observations of the electric field.

Cumnock et al. [1992] studied the ionospheric plasma flow as measured by the DMSP F8 satellite under the northward IMF period. In the southern (summer) hemisphere they found clear evidence for four-cell convection and were able to identify how these cells evolved as a function of the IMF B_y. This event was further studied by *Freeman et al.* [1993], who found that in the northern (winter) hemisphere under northward IMF conditions the convection patterns were not well defined and the flows were very irregular. In contrast, under southward IMF conditions, the standard two-cell convection pattern existed in both hemispheres with very similar magnitudes of electric field. They found that under strongly southward IMF conditions the cross-tail magnetospheric potential (as inferred from ionospheric measurements) exceeded 180 kV. However, under northward IMF conditions the four-cell southern hemisphere convection pattern had a reversed polarity and a cross-tail potential of up to 80 kV, while in the northern hemisphere the cross-tail potential did not reverse polarity and fell to a few tens of kV. *Farrugia et al.* [1993] studied the distribution of substorms during this magnetic cloud passage. No substorms were found during the first 16 hours, the period of northward IMF. Then a total of 23 substorms were found in the following 20 hours. This included at least two in the time immediately following the cloud passage. These substorms all occurred during the magnetic storm period.

Knipp et al. [1993, 1994] used the AMIE technique to model the convection electric field in both hemispheres during this event; extensive observations were made by satellites of the ionospheric plasma flow and by radars (both coherent and incoherent) of the plasma flow and of ionospheric currents by ground-based magnetometers. Then using conductivity models based on empirical patterns and satellite measurements of the auroral precipitation the AMIE technique generated electric

[1]Center for Atmospheric and Space Sciences, Utah State University, Logan.

[2]Plasma Physics Division, Naval Research Laboratory, Washington, DC.

[3]Institute for Computational Sciences and Informatics, George Mason University, Fairfax, Virginia.

[4]Air Force Research Laboratory, Space Effects Division/GPSM, 29 Randolph Road, Hanscom AFB, Massachusetts.

Paper number 98JA01744.
0148-0227/98/98JA-01744$09.00

potential patterns in the auroral and polar ionospheres. Under the most disturbed conditions these patterns reached below 50° invariant latitude. Because of the slowly changing IMF conditions during the 30-hour cloud passage, the AMIE electric field patterns vary quite systematically during the northward IMF conditions. Under southward conditions the pattern is dominated by the standard two-cell convection, but these are dynamically modified by the recurrence of substorms. These substorms are typically separated by 50 min during the southward IMF period. The results of these AMIE calculations are in good agreement with previous studies of this event that considered the magnetospheric response to the magnetic cloud passage. The magnitudes of the cross-tail potentials were somewhat smaller from the AMIE patterns than those deduced directly from the DMSP-F8 dawn-dusk orbits, i.e., > 120 kV as opposed to > 180 kV at the storm peak [*Knipp et al.*, 1993].

Another technique that generates or simulates the magnetospheric electric field is a magnetospheric magnetohydrodynamic (MHD) model. Using the Naval Research Laboratory (NRL) MHD simulation model of the solar wind-magnetosphere interaction [*Fedder and Lyon*, 1995], *Chen et al.* [1995] modeled the magnetospheric response to an idealized magnetic cloud passage. The same simulation model was applied to the January 14, 1988, magnetic cloud passage event [*Slinker et al.*, 1995]. Through this type of simulation the electric field at the lower, or inner, boundary of the MHD model can be mapped down into the ionosphere along magnetic field lines. Thus patterns in the same coordinate frame as those provided by the previous studies are obtained; indeed these MHD patterns have been compared with the AMIE patterns with good overall agreement [*Slinker et al.*, 1995]. The slowly varying IMF conditions make this period ideal for such comparisons since on time scales needed to average data (a few min for AMIE) and to reach quasi-equilibrium conditions (tens of minutes for MHD) the IMF is approximately constant.

In this study the extensive knowledge of the magnetospheric electric field, and to a lesser extent the electron precipitation, is used to drive an ionospheric model. For this initial study the summer southern hemisphere is modeled because in this hemisphere the electric field patterns were observed to be well defined at all phases of the magnetic cloud passage. This simulation is then compared with climatological ionospheric simulations in which geomagnetic indices and solar wind parameters have been used to select empirical electric field and precipitation patterns. Satellite observations of plasma density in the topside ionosphere are used as a reference against which the model simulations are compared. The ionospheric and magnetospheric models are discussed in section 2. A review of the storm period centered on January 14, 1988, is given in section 3 with thermal electron density observations during this period being shown in section 4. Model simulation results are presented in section 5, while a comparison of these results with the observations is given in section 6. A discussion (section 7) and a conclusion (section 8) follow.

2. Models

In this study the ionospheric response to magnetospheric forcing is simulated using the Utah State University time-dependent ionospheric model (TDIM). The magnetospheric forcing is generated in two distinct ways. First, the electric field and electron precipitation patterns are obtained from the MHD simulation for January 14, 1988, based on the Naval Research Laboratory Magnetohydrodynamic (MHD) model. Second, the magnetospheric forcing is obtained from empirical models of the electric field and auroral precipitation which have been selected based on geomagnetic indices and solar wind parameters.

2.1. Ionospheric Model

The TDIM ionospheric model was initially developed as a midlatitude, multi-ion (NO^+, O_2^+, N_2^+, and O^+) model by *Schunk and Walker* [1973]. The time-dependent ion continuity and momentum equations were solved as a function of altitude for a corotating plasma flux tube including diurnal variations and all relevant *E* and *F* region processes. This model was extended to include high-latitude effects due to convection electric fields and particle precipitation by *Schunk et al.* [1975, 1976]. A simplified ion energy equation was also added, which was based on the assumption that local heating and cooling processes dominate (valid below 500 km). Flux tubes of plasma were followed as they moved in response to the convection electric fields. The addition of plasma convection and particle precipitation models is described by *Sojka et al.* [1981a, b]. *Schunk and Sojka* [1982] extended the ionospheric model to include ion thermal conduction and diffusion thermal heat flow. Also, the electron energy equation was included by *Schunk et al.* [1986], and consequently, the electron temperature is now rigorously calculated at all altitudes. The theoretical development of the TDIM is described by *Schunk* [1988], while comparisons with observations are discussed by *Sojka* [1989].

In addition to the physical processes built into the model, the TDIM requires several inputs. The magnetospheric inputs for the TDIM are the auroral precipitation and convection electric field. Typically, the auroral electron precipitation has been obtained from the *Hardy et al.* [1987] model, and the convection has been obtained from the *Heppner and Maynard* [1987] models. The computer algorithm for the Heppner and Maynard convection model was developed at the Air Force Research Laboratory (AFRL) at Hanscom AFB (F. Rich, private communication, 1990). The MSIS-86 model is used to represent the neutral atmosphere [*Hedin*, 1987], while the neutral wind is represented by the *Hedin et al.* [1991] HWM 90 model.

In one part of this study, output from the Naval Research Laboratory (NRL) MHD magnetosphere model is used to drive the TDIM. Hence the question of interface is reduced to matching the magnetospheric convection and precipitation to the TDIM inputs. Of note is that neither of these inputs or outputs are based on regular grids. The TDIM uses a Lagrangian technique, where plasma flux tubes are followed as they move through the neutral gas. Hence the TDIM requires electric field and electron precipitation inputs at arbitrary locations within the high-latitude ionosphere. Normally, the high-latitude ionosphere is defined as magnetic dipole latitudes poleward of 40° (occasionally poleward of 50°). This lower latitude is determined by the requirement that the *F* region must be corotating at this most equatorward location. Consequently, no boundary condition needs to be developed for *F* region plasma leaving or entering the model at the equatorward boundary. Typically, this latitude would be several degrees equatorward of the equatorial edge of the diffuse auroral precipitation at midnight. In addition to the spatial

requirements, there are also timing requirements. The TDIM solves the continuity, momentum, and energy equations dynamically with variable time steps that are determined by solar and geophysical conditions. During substorm activity, the time step could be as short as 10 s, but more typically it is of the order of tens of seconds, and it increases to minutes at corotating midlatitude locations during quiet geomagnetic conditions.

2.2. Magnetospheric Model

The NRL MHD model of the magnetosphere has been described in detail by *Fedder and Lyon* [1995] and *Fedder et al.* [1995a]. The model solves the ideal MHD equations for the solar wind and the outer magnetosphere (beyond 3.5 R_E). A nonorthogonal adapted mesh is used, which maximizes the spatial resolution at the magnetopause, in the ionosphere, and in the geomagnetic tail. By using a time step of less than 1 s, the model is able to describe unambiguously the propagation of fast waves on the mesh. *Fedder and Lyon* [1987] have shown that the model simulates the important process of magnetic merging in such a way that the reconnection rate is determined by the physical conditions of the solar wind and the conductivity of the ionosphere, with the simulated reconnection rate being insensitive to the numerical mesh size.

Of specific relevance to this study is the question of how the MHD model's inner boundary at 3.5 R_E is determined. *Fedder et al.* [1995a] and prior researchers matched the inner boundary to a line-tying ionosphere, in the sense of *Coroniti and Kennel* [1973], and used a uniform conductance of 5 mhos. A more realistic inner boundary condition was developed by *Fedder et al.* [1995b], in which the ionospheric conductance is given by a parameterized empirical model of both the solar EUV and auroral precipitation ionization sources. The procedure involves using parameters in the innermost MHD mesh points to compute the field-aligned electric potential which in turn leads to the characteristic energy of the precipitating electrons and the precipitating flux from the field-aligned current. The major improvement resulting from these parameters is that a dynamic auroral conductance is obtained. *Fedder et al.* [1995b] demonstrate that in order to obtain the auroral dynamics observed by the Viking satellite and the ionospheric currents inferred from the auroral A indices, the parameter selection for these ionospheric-MHD inner boundary empirical algorithms is of key importance. At this time, no feedback exists from the TDIM to the NRL MHD simulation.

Interfacing the MHD output fields of electric field and electron precipitation was discussed at length by *Sojka et al.* [1997] and *Bowline et al.* [1996] in the first TDIM-MHD study. The MHD model generates solutions every few tenths of a second which is considerably more frequent than the TDIM. Hence the temporal coupling is a matter of the TDIM selecting the appropriately timed MHD solution. The spatial interface is not as simple. The MHD output is an irregular grid in the ionosphere with roughly 400-km resolution. In contrast, the TDIM simulation output grid is an almost uniform 80 × 80 km grid, whereas the input to the TDIM is not a grid but needs to be a continuous function because the TDIM follows plasma flux tubes in a Lagrangian manner. Hence an interpolation technique is used to determine the electric field and electron precipitation over a continuous range of latitudes and longitudes. At this time, no feedback exists from the TDIM to the NRL MHD simulation.

3. January 14, 1988, Magnetic Cloud Passage Event

Since a large body of research has been published on this event, especially its solar wind and magnetospheric attributes, these details are not repeated here beyond the summary in the introduction. Figure 1 shows the history of four key parameters during January 14, 1988. The IMF B_y and B_z components as monitored by the IMP 8 satellite are shown in the top two panels. Apart from a data gap between 0100 and 0400 UT the IMP 8 data set is continuous through the passage of the magnetic cloud. The cloud is first encountered at about 0000 UT with the IMF B_z going northward and reaching a maximum northward value of over 20 nT at about 1000 UT; after which B_z systematically rotates southward. It crosses zero at 1600 UT and continues southward reaching -20 nT at about 2100 UT. The IMF B_z then continues to rotate back to zero at about 1000 UT on January 15, 1988. Hence the passage of the cloud takes about 32 hours. The IMF B_y component also undergoes a systematic rotation from positive to a longer period of negative; see top panel of Figure 1. More detailed discussions of the IMP 8 observations and the magnetic cloud are given by *Freeman et al.* [1993].

From the ionospheric response point of view the lower two panels of Figure 1 show how storm energy is being deposited. The *Dst* index shows that during the northward IMF period from 0000 to 1600 UT conditions are relatively quiet with a magnetic storm beginning at about 1600 UT as the *Dst* rapidly decreases reaching -150γ by 2300 UT. A magnetic storm of this magnitude will lead to significant energy deposition in both the ionosphere and thermosphere. This energy deposition is associated with the enhanced magnetospheric electric fields and auroral precipitation that occur during this period. Both these energy sources scale with the *Kp* index, which is shown in the lower panel of Figure 1, and a previous simulation has shown that the precipitating energy is proportional to the square of the cross-polar potential [*Chen et al.*, 1995]. Since *Kp* is a 3 hourly index it lacks time resolution in tracking the growth phase of the magnetic storm from 1600 to 2300 UT. However, the increasing *Kp* trend is consistent with the storm evolution.

The *Kp* index does however indicate that the 0000-1600 UT period is in fact not entirely a quiet period. At the time of most northward IMF the *Kp* is at its lowest of 2. A *Kp* of 2 is not quiet, implying a significant electric field still exists. Indeed, the early period of northward IMF, 0000 to 0600 UT is associated with *Kp* values of 4 and 5, which are quite disturbed conditions. Hence, even in this long period of northward IMF the magnetosphere has not dropped to a quiet state.

Above the top panel in Figure 1 are a set of 6 numbered event markers with their associated UTs. These six times are referred to repeatedly in this study as key phases of the magnetospheric driver morphology as well as ionospheric response morphology. Results of the ionospheric simulations will be shown in subsequent figures at these times. Markers 1, 2, and 3 show the ionospheric evolution toward the most northward IMF condition, marker 4. The start of the storm growth phase is shown by marker 5, while the ionospheric storm conditions are represented by marker 6.

4. Ionospheric Observations

The Defense Meteorological Satellite Program (DMSP)-F8 polar orbiting satellite made continuous observations of the

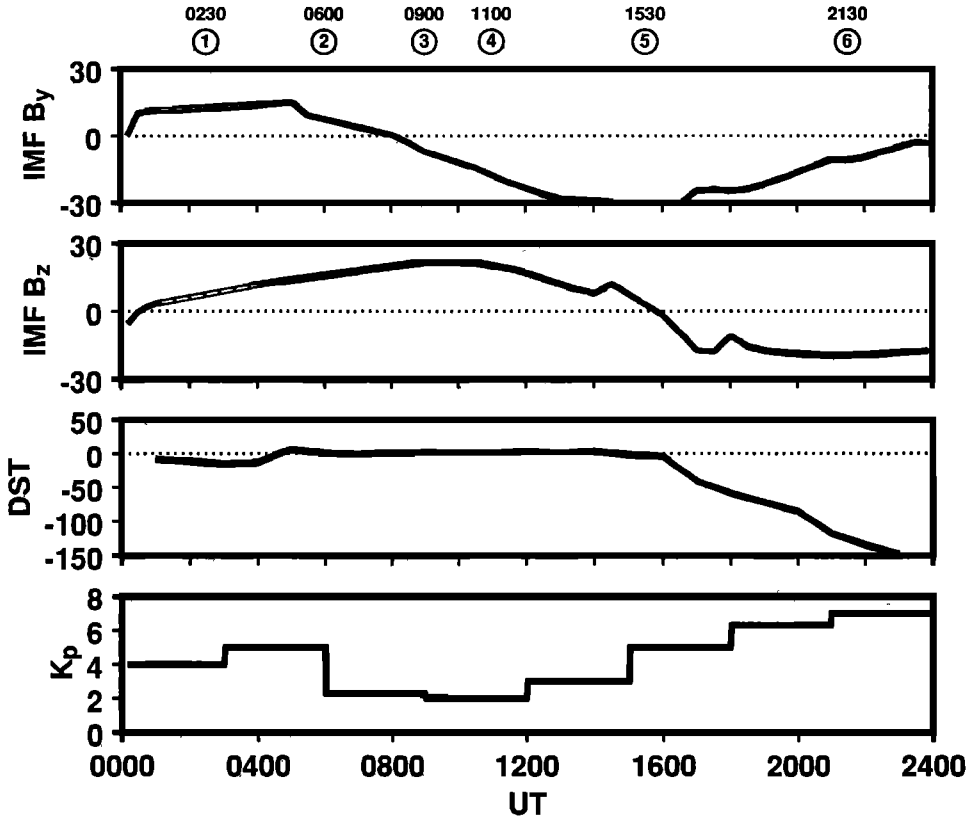

Figure 1. Geomagnetic *Kp* and *Dst* indices, and the IMF B_z and B_y components, on January 14, 1988. Selected universal times are indicated and labeled at the top for reference throughout the paper. The IMF data gap in the B_z and B_y components is shown by the dashed line from 0100 to 0400 UT.

topside ionosphere during January 14, 1988, with the SSIES plasma sensor. The F8 satellite is in a Sun-synchronous dawn-dusk orbit at an altitude of 840 km. Because of the Earth's rotation and the offset of the magnetic dipole axis from the rotation axis, the satellite trajectory changes from orbit to orbit in the magnetic frame. This variation of the F8 orbit on January 14, 1988, in the southern hemisphere is shown in Figure 2. For clarity, Figure 2 has been split into two magnetic polar plots so that orbit paths do not overlap. Each orbit path is labeled with the corresponding UT as the satellite crosses the noon-midnight meridian. During the 24-hour period the satellite passes very near to the magnetic pole at about 0800 UT and again at 2320 UT, while around 1630 UT it is equatorward of the cusp, missing the magnetic polar cap altogether. Table 1 lists the adopted orbit number scheme for this study along with the corresponding UT shown in Figure 2 and a cross reference of orbit number and UT with the event markers identified on Figure 1.

In situ electron density measurements from the SSIES sensor are used in this study. The special sensor for ions, electrons and scintillation (SSIES) package of instruments on DMSP is described by *Rich and Hairston* [1994]. Electron density measurements at one second intervals are available along the 14 orbit tracks shown in Figure 2. In order to present this data set in a compact form, these densities are color coded and displayed in a relative trajectory distance versus orbit number; see Plate 1. Each orbit's data run from left to right as a horizontal strip. The strip is plotted as a function of relative distance along the orbit referenced to the location at the center of the x axis when the satellite crosses the magnetic noon-midnight meridian on that orbit. Data are plotted only for magnetic invariant latitudes greater than 58°. For example, the strip for orbit 9 is relatively short, because orbit 9, at 1450 UT, misses the magnetic polar cap (see Figure 2) and spent a relatively short time above 58° invariant latitude. The invariant latitude limit of 58° is chosen to correspond to the lowest latitude of the MHD simulation and hence defines the region of relevance for model data comparisons.

In Plate 1 the logarithm of the observed electron density at 840 km is color coded over 1.5 orders of magnitude. The 1-s electron density observations have been averaged over 20-s before being plotted. This 20-s average corresponds to about 160 km along the satellite track, which closely matches the TDIM output resolution of 80 × 80 km. For most of the prestorm, before 1600 UT, the density variations are systematic from orbit to orbit and relatively unstructured with densities ranging from 10^4 to 10^5 cm^{-3}. The highest densities are found at the lowest latitudes. From orbits 7 to 9 the entire "polar cap" has densities reaching 4×10^4 cm^{-3}. However, this is the time period when the F8 orbit is just glancing the polar cap and could be in the dayside cusp region. As the storm develops from orbits 9 to 11, an enhanced density is observed in only the dusk sector with low densities in the dawn sector. During the storm orbits 12, 13, and 14, an enhanced density is found only in a restricted region of about 500 km inside the polar cap. Elsewhere the densities are significantly depleted. Since orbit 14 occurs almost 24 hours after orbit 1, these two orbits are located in approximately the same place and can be compared to demonstrate the effects of the storm. The storm growth enhancement associated with the dusk sectors of orbits

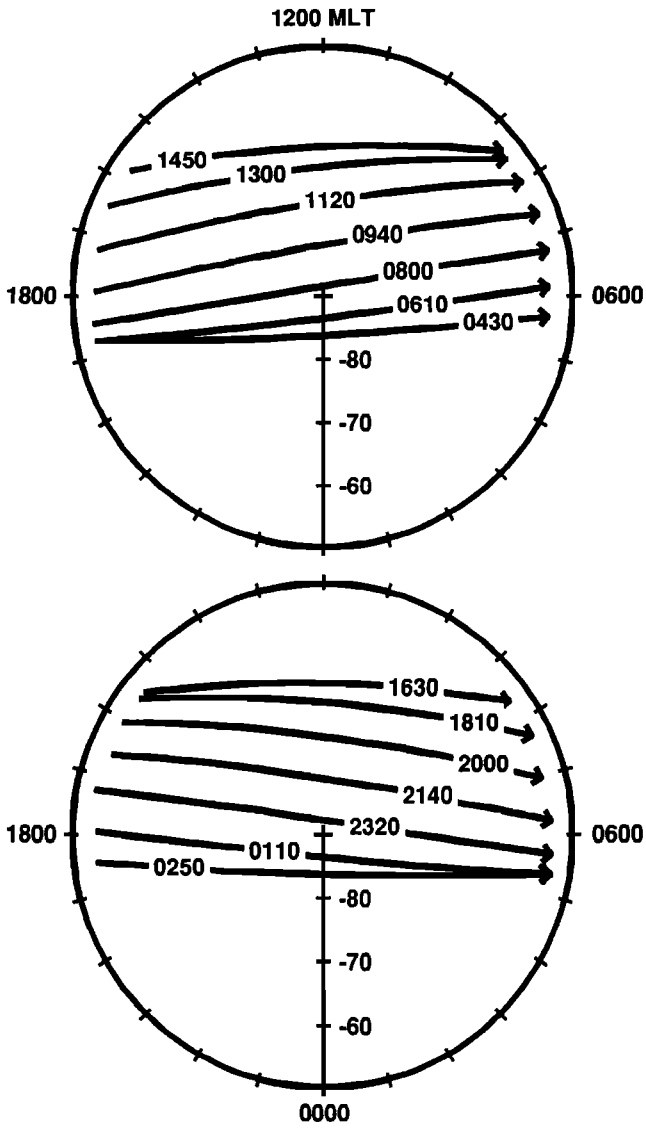

Figure 2. Fourteen DMSP-F8 satellite orbit paths across the southern hemisphere on January 14, 1988, are shown in magnetic latitude–MLT polar plots. Each orbit is labeled with the approximate UT of its southern polar passage.

7 to 11 is probably the Storm Enhanced Density (SED) effect reported by *Foster* [1993]. The narrow regions of enhanced densities found in the polar cap on orbits 12, 13, and 14 are probably cross sections of the tongue of ionization. The presence of these marked density features is very significant when taken in the context that the southern polar cap is in sunlight during this event, i.e., January 14 is summer in the southern hemisphere.

5. TDIM Simulations

The TDIM was run twice with different magnetospheric inputs for the January 14, 1988, magnetic cloud passage event. In both simulations the magnetospheric electric field and electron precipitation were varied in a manner intended to represent the magnetospheric response to the event. In the first study the electric field and electron precipitation were obtained from the NRL MHD model simulation of this event. In the second study a standard empirical approach was adopted whereby the electric field was represented by *Heppner and Maynard* [1987] convection patterns chosen according to the changing *Kp* and IMF B_y and B_z conditions; and electron precipitation was derived from the *Hardy et al.* [1987] model according to the *Kp* index. During the event these indices and solar wind parameters are slowly changing, hence it can be argued that snapshot empirical patterns may be reasonably representative of the prevailing conditions.

Figure 3 shows equipotential contour plots of six magnetospheric electric fields (with corotation added) for the MHD inputs (Figure 3a) and empirical inputs (Figure 3b). The times of the six snapshots (panels) are those of the six event markers identified in Figure 1 and Table 1. The equipotential contours, which are spaced at 10-kV intervals, correspond to plasma flow trajectories, or at least the instantaneous flow pattern. The general circulation directions have been identified by arrows on some of the trajectories; this is particularly necessary for identifying a region of sunward convection in the polar cap that moves across the pole from dawn toward dusk in the 0600 to 1100 UT period. The MHD convection pattern exhibits this feature most clearly, although the statistical patterns do have a polar cap sunward flow region that also crosses the polar region from dawn to dusk. This dawn to dusk drift can best be seen by focusing on the large counter clockwise flowing dawn cell in panel 1 of Figure 3; in panel 2 this cell occupies the center of the polar cap, and by panel 3 it has moved into the dusk sector, while in panel 4 it has disappeared altogether. However, the overall convection circulation morphologies are quite dissimilar between the two models during the northward IMF periods, panels marked 2, 3, and 4.

During southward IMF conditions the difference between the models is more a matter of the cross polar cap potential magnitude which is similar to a difference in electric fields and hence $|\mathbf{E} \times \mathbf{B}/B^2|$ speeds. At 1530 UT, panel marked 5, the IMF B_z is just turning southward but the B_y component is strongly negative; a strong two-cell pattern has developed. The orientation of the two cells relative to the noon-midnight meridian is consistent with strong IMF B_y given that the patterns are in the southern hemisphere. The MHD pattern has a cross polar cap potential of 240 kV whereas the *Kp*-driven

Table 1. DMSP-F8 Orbits on January 14, 1988

Orbit Reference Number	Southern Hemisphere, UT	Snapshot * Event Number
1	0110	---
2	0250	1
3	0430	---
4	0610	2
5	0800	---
6	0940	3
7	1120	4
8	1300	---
9	1450	5
10	1630	---
11	1810	---
12	2000	---
13	2140	6
14	2320	---

*These times were not selected to correspond to an F8 orbit but rather a geomagnetic condition.

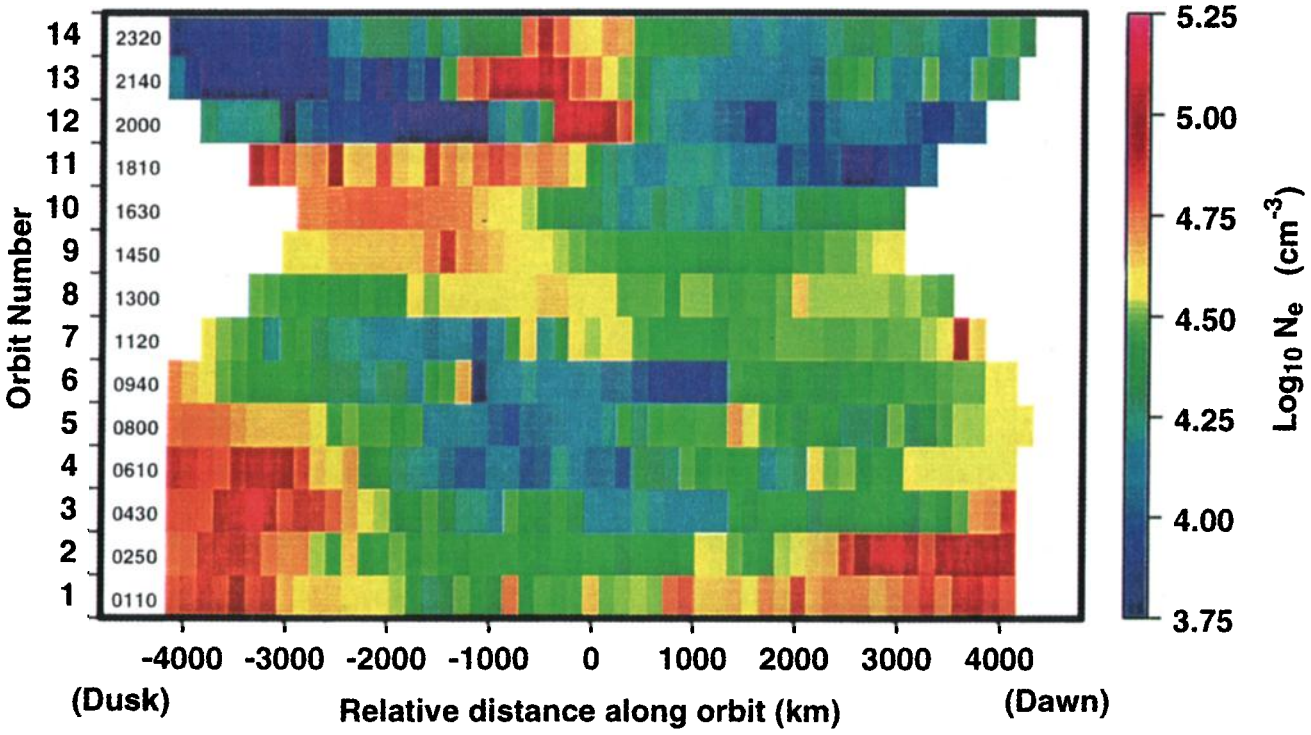

Plate 1. Summary of DMSP-F8 electron density measurements on January 14, 1988, in the southern hemisphere poleward of 58° invariant latitude. Orbits are stacked with UT increasing upwards on the vertical axis. Horizontally each orbit is centered at its magnetic noon-midnight crossing which is labeled zero on the relative distance axis. The measured electron density is averaged over 20 s and color coded on a logarithmic scale.

empirical pattern has only 52 kV. This difference is further magnified at 2130 UT, well into the expansion phase of the geomagnetic storm.

The low values of cross polar cap potential for the Heppner and Maynard patterns are a consequence of using a climatological model developed for $Kp = 3^+$ conditions being scaled by a 3 hourly Kp index (see Figure 1). The simple scaling relationships based on statistical studies using a 3 hourly index can hardly reach 100 kV. During this storm period the DMSP satellite observed potential drops along the satellite track that reached values over 200 kV which implies the peak potential drop was probably larger. These magnitudes are still somewhat lower than those simulated by the MHD model. This question of reconciling the polar cap potential pattern is currently being studied by a team of DMSP-AMIE-NRL MHD scientists (J. Fedder, private communication, 1998).

Morphological differences between the MHD and empirical models are found for the electron precipitation shown in Figure 4. During the transition from IMF B_z zero to strongly northward, panels marked 1 to 4, the two models evolve differently. The MHD auroral oval reduces to energy flux levels below the lowest grey scale shade, 0.25 erg cm^{-2} s^{-1} as the IMF goes northward and a region of weak precipitation is found in the polar cap. This trend is not present in the empirical model since that model was developed as an average model over all IMF orientations. The presence of weak precipitation in the polar cap is not inconsistent with IMF northward conditions. During the southward IMF period represented by panels marked 5 and 6, the conventional oval dominates although there are still significant differences between the two models. At 2130 UT, in the storm the MHD model has a peak electron precipitation flux of 5.9 erg cm^{-2} s^{-1}, while the statistical oval reaches 8.6 erg cm^{-2} s^{-1}. Both energy flux maxima occur in the postmidnight sector around 0100 MLT at 65° and 60° invariant latitude for the MHD and Hardy cases, respectively.

The simulated F region peak density (N_mF_2) and height (h_mF_2) are shown color coded in Plates 2 and 3 in the same format as the inputs in Figures 3 and 4. The first panel at 0230 UT is sufficiently far into the simulation period, which began at 0000 UT, that these densities are not sensitive to the initial simulation densities. This is because the polar ionosphere is in sunlight and hence the time for the F region ionosphere to come into dynamic equilibrium with the electric field and auroral drivers is somewhat shorter than the usual 5 to 6 hours in winter. The initial conditions were computed for the two separate 0000 UT conditions respectively for the two simulations. These were for Kp 4 disturbed conditions indicating that even in sunlight at 0000 UT the two initial conditions were different. During the following 2.5 hours these initial differences were to a large extent overridden by the different electric fields and auroral precipitation patterns in the two simulations. Hence the difference in the first panel of the two simulations is mainly the result of differences in their respective first 2.5 hours of magnetospheric inputs. This dependence upon the inputs shown in Figures 3 and 4 holds for all the TDIM results presented in Plates 2 and 3. The MHD-driven TDIM simulation has resulted in considerably lower polar cap densities. Plate 3 compares the MHD driven TDIM versus the empirically driven TDIM, i.e., the top six panels with their corresponding panel in the bottom six. During the

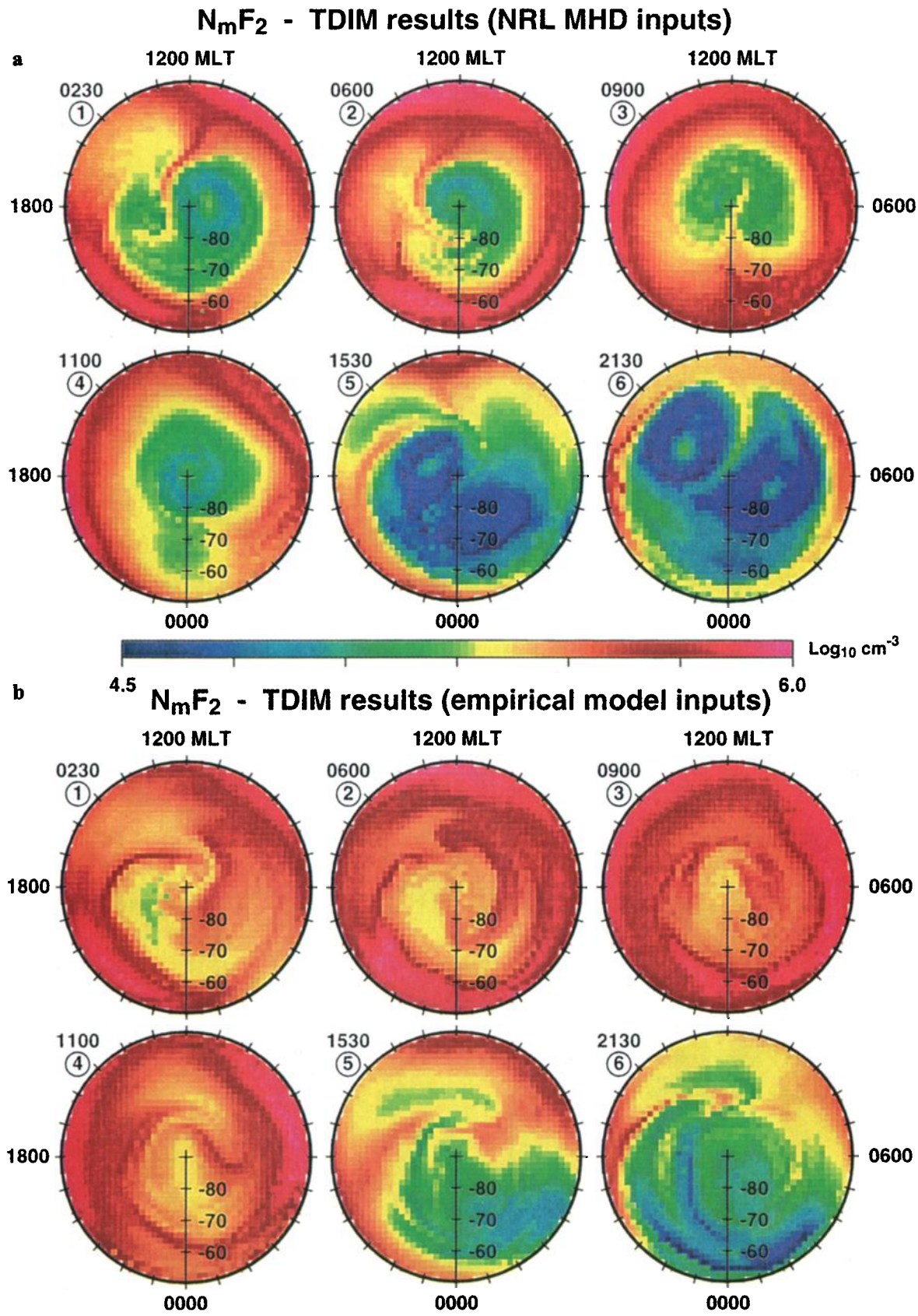

Plate 2. Comparison of TDIM N_mF_2 results based upon (a) NRL-MHD inputs and (b) empirical inputs. Snapshots are shown at the six selected UTs identified in Figure 1.

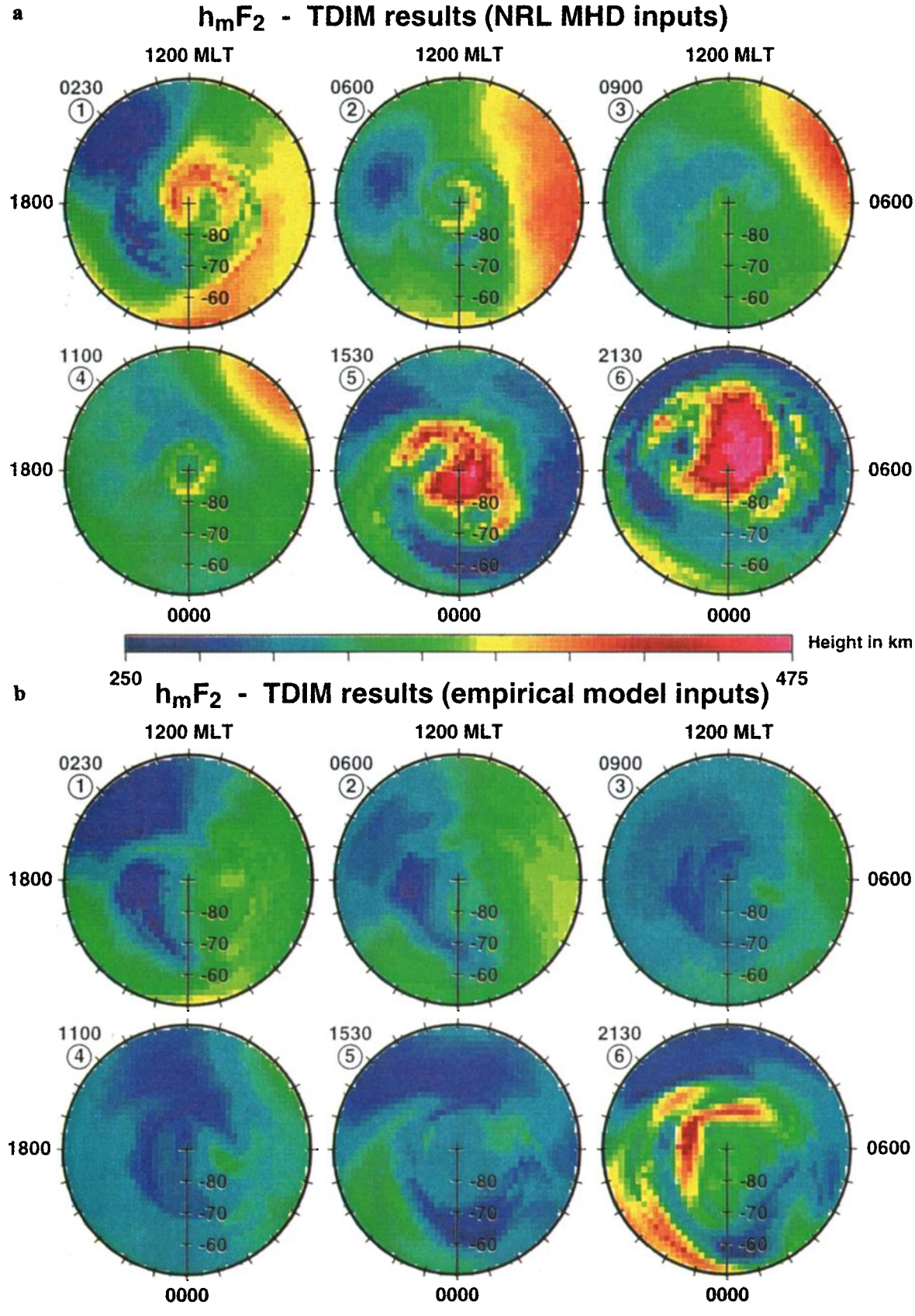

Plate 3. Comparison of TDIM h_mF_2 results based upon (a) NRL-MHD inputs and (b) empirical inputs. Snapshots are shown at the six selected UTs identified in Figure 1.

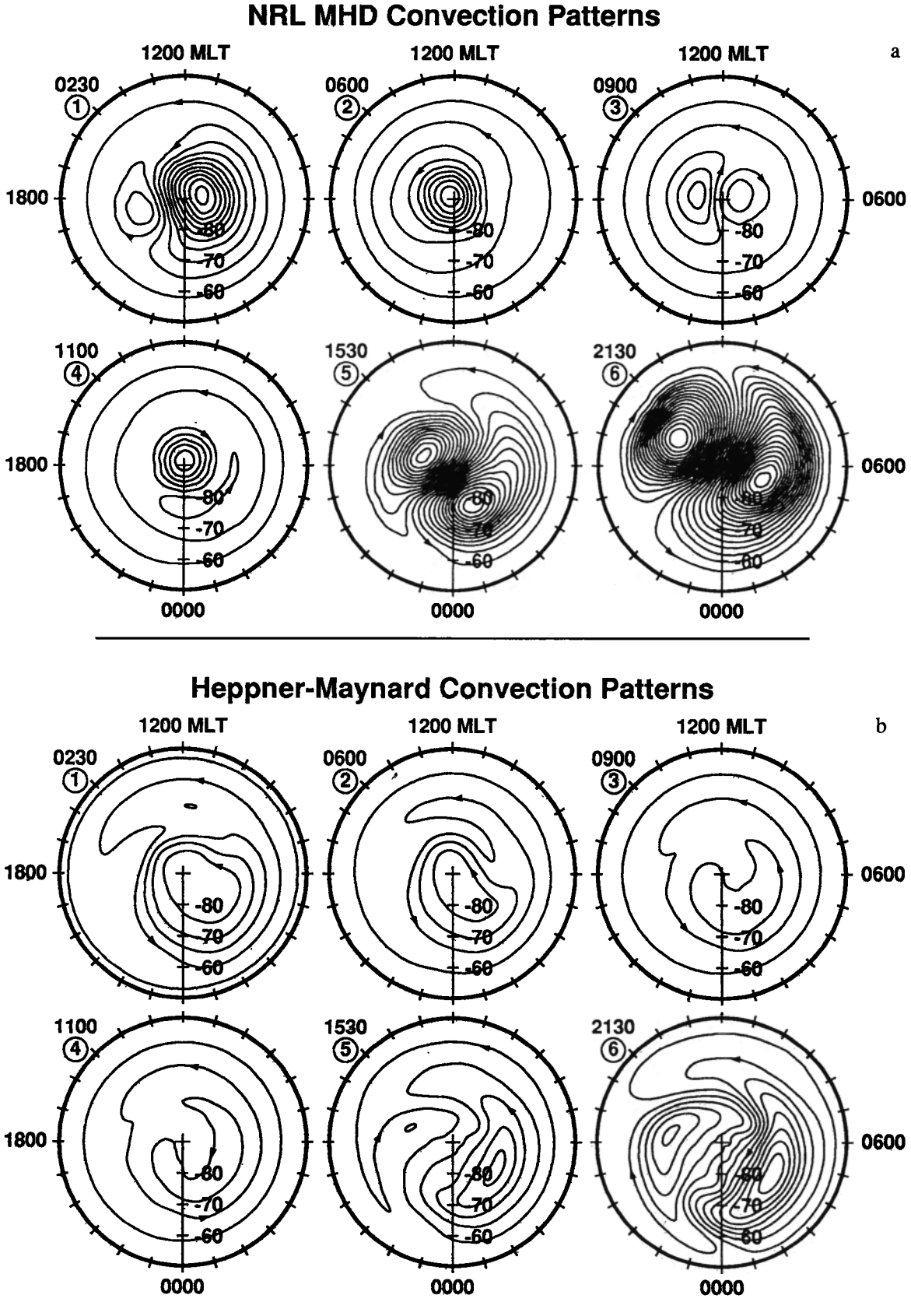

Figure 3. Comparison of electric potential patterns with corotation added, for the (a) NRL-MHD model with (b) the empirical Heppner and Maynard model. Snapshots are shown at the six selected UTs identified in Figure 1. The electric potential contours are shown at 10-kV intervals. The direction of plasma flow is indicated by arrows on certain of the equipotential contours.

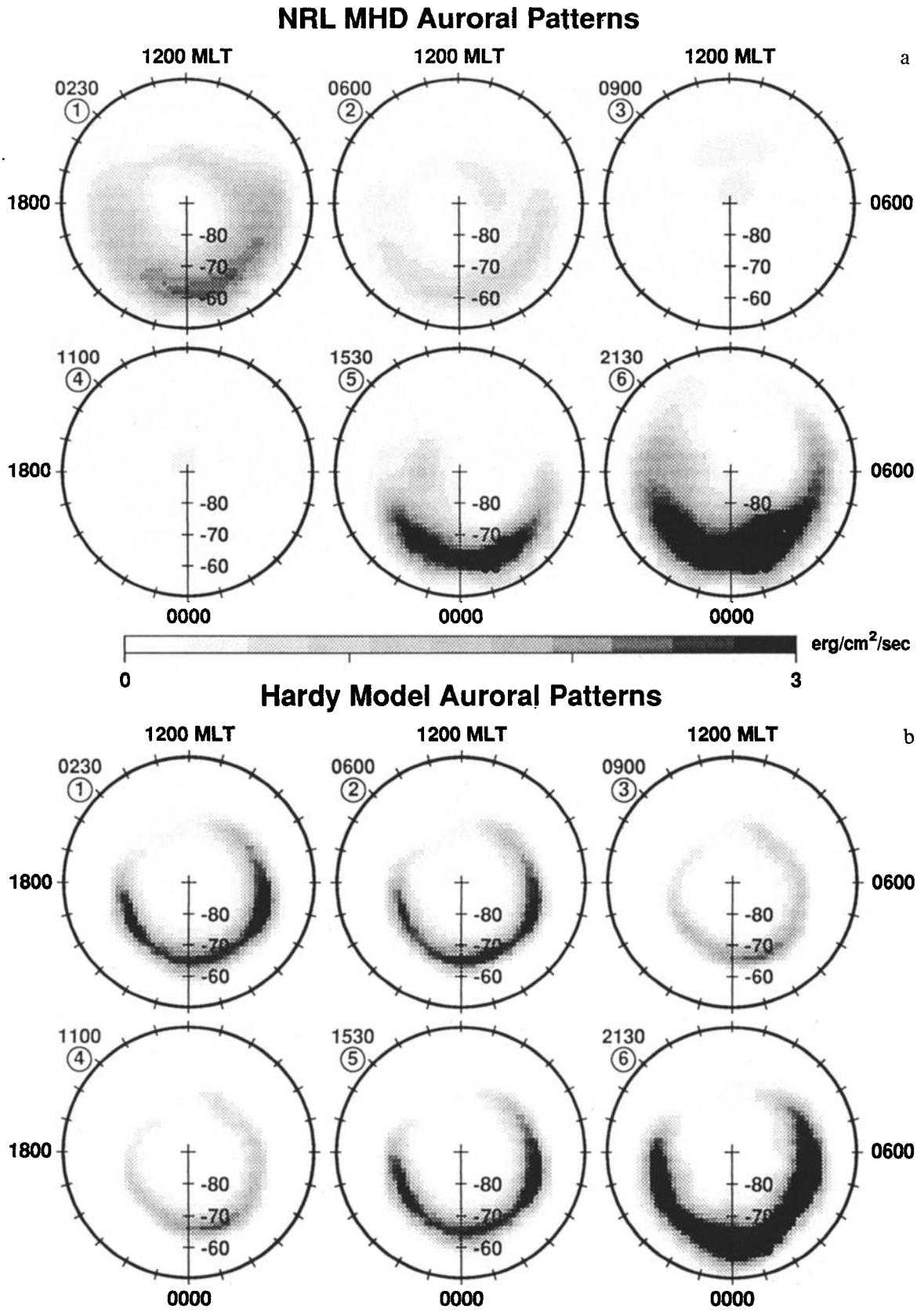

Figure 4. Comparison of electron precipitation energy flux patterns for (a) the NRL-MHD model with (b) the empirical Hardy model. Snapshots are shown at the six selected UTs identified in Figure 1.

northward IMF period, in the vicinity of the magnetic pole, N_mF_2 decreases to below 10^5 cm^{-3} for the MHD case and only to 2×10^5 cm^{-3} for the empirically driven case. Note that in this simulation the polar cap is in sunlight; hence these relative depletion levels are quite significant. The source of the extra depletion is due to the enhanced convection in the MHD case leading to higher ion temperatures and consequently faster recombination rates. An alternative mechanism would be associated with a lifting or lowering of the F layer; however, Plate 3 shows h_mF_2 to be higher in the MHD case, while a density depletion would more likely be associated with a lowering of h_mF_2. In the IMF southward turning storm phase, panels marked 5 and 6, the F layer over the polar cap is further depleted. The largest depletions are again found in the MHD case, with densities falling well below 3×10^4 cm^{-3}. For the empirically driven simulation the corresponding densities remain above 6×10^4 cm^{-3}. This storm feature difference is readily attributed to the enhanced electric fields; see Figure 3, panels 5 and 6. The MHD electric fields are significantly larger than the empirical ones, leading to greater heating and density reduction in the MHD case. Midlatitude densities are found to be similar for the two simulations since corotation is almost always dominant in this region, although the MHD and empirical storm convection patterns at the end of the simulation are encroaching on this lower latitude.

Both simulations produce various "weather" fine structure features. The MHD case develops a well defined tongue of ionization (TOI) in panels 1, 2, 3, 5, and 6 of Plate 2. A TOI is usually viewed as the feature resulting from high density dayside plasma convecting through the cusp into a dark polar cap, although in this study the entire region is sunlit. However, as has already been shown in section 4, during this storm a TOI is observed by the DMSP-F8 satellite. The TOI in the MHD case for panels marked 1, 2, 5 and 6 is consistent with the idea of high-density dayside plasma being swept through the cusp into the polar cap. However, the TOI in panel 3 does not follow this morphology; it is associated with the sunward convection across the middle of the polar cap (see Figure 3 MHD panel 3). This is a new TDIM feature, a reverse-flow TOI. The origin of the higher densities is in fact still dayside high-density plasma that has convected around the pair of reverse convection cells in the center of the polar cap. On reaching the midnight sector this plasma has been swept sunward across the polar cap forming the TOI. Looking at Plate 2, MHD panels 1 and 2 leading to the reverse flow TOI, one can see how the original TOI drapes around the low density polar hole associated with the duskward moving reverse convection cells. In fact, MHD panel 2 almost shows the full flow history of the original TOI into a reverse flow TOI as it drapes over the dusk edge of the polar hole towards midnight. The convection geometry shown in the empirical patterns, Figure 3 panels 1, 2, and 3, would not bring the TOI back into the polar cap at midnight and hence would not be expected to generate this unusual reverse-flow TOI from a dusk sector draped TOI. However, it might be possible from a TOI that drapes around the dawn sector. Indeed such a feature is developed but does not show a particularly clear TOI signature; rather the high density filaments tend to straddle many convection paths rather than follow one path.

6. DMSP-TDIM Comparisons

Given that the two simulations are quite dissimilar in their F layer morphologies, the question to be addressed is: does either come close to the real-world observations? The simulation results need to be compared with the 14 orbits of DMSP-F8 electron density at 840 km discussed in section 4. To do this, TDIM simulations need to be carried out along the 14 DMSP-F8 orbit paths shown in Figure 2. Plate 4 shows the comparison for orbit 13 (2140 UT), corresponding to the event mark 6 of Figures 1, 3, 4 and Plates 2 and 3. As already mentioned in section 4, this is the time during the storm phase when DMSP-F8 encountered a narrow enhanced density region, or TOI, in the polar cap. The MHD-TDIM simulation, Plate 2 top panel 6, also shows a well-defined TOI flowing into the depleted polar hole. In Plate 4, the top left dial plot shows the electron density at 800 km which can be compared with the corresponding N_mF_2 (top, panel 6) in Plate 2. At 800 km the TOI is well defined and flows deep into the polar cap, while on the dayside the densities do not appear enhanced. This is because the density at 840 km depends not only on the N_mF_2 values below but also on the topside scale height (the plasma temperature). Hence, in the polar cap a region of very high flow exists leading to higher temperatures and hence relatively enhanced densities at 840 km. These ion temperatures range from 1000 to 1500 K from the bottomside to topside F region under quiet geomagnetic conditions. Under the disturbed conditions the ion temperature is elevated, ranging from 4000 to 6000 K near the F region peak and from 3500 to 4700 K at 800 km. Furthermore, because of the strong low-altitude friction heating, the altitude variation is inverted from the usual cold bottomside to hot topside. The path of the F8 satellite is shown on the electron density dial plots in Plate 4 as an arrow. A comparison of the electron density along the path is shown in the bottom panel of Plate 4. Both the observations (cross) and MHD case (red line) show a depleted polar cap with a TOI in the middle. These two data sets have almost the same dynamic range and apart from a shift in location of TOI can be considered a good equivalence. This is especially the case when they are contrasted with the relatively featureless empirically driven simulation (green line). In fact, the major feature in this case is an enhanced density in the dusk sector that corresponds to a SED [*Foster*, 1993] in the afternoon sector.

Plate 5 shows all 14 orbits of simulated TDIM data for the MHD case (Plate 5a) and empirically driven case (Plate 5b), plotted in identical format to the F8 observations in Plate 1. Comparing the prestorm northward IMF periods, orbits 2 through 7, one finds qualitative similarities between all three plots and distinct differences. In the low-latitude regions the density is higher while the polar caps are depleted. The observations show a somewhat more extended higher-density dusk sector, while both models show the dawn sector to be higher. The dynamic ranges agree very well, from 10^4 to just over 10^5 cm^{-3}. The MHD (Plate 5a) differs from the observations in Plate 1 in two distinct ways. First, between orbits 1 and 4 there is a high-density ridge feature that extends from the central polar cap at orbit 0 to dusk low latitudes by orbit 4. This feature could in part be a remnant fossil TOI that was created by the initial MHD electric field pattern since we lacked information about the IMF prior to 0000 UT. A second difference is the dawn sector lowest latitudes region between orbits 3 and 6 which have very high densities in the TDIM model (Plate 5a) and yet much lower densities in the observed case, Plate 1. In the TDIM case these high densities have convected round the night side from the post afternoon sector. This took more than 12 hours since these flux tubes are corotating. Again, this puts the early time history of this

region at a time prior to the simulation start when poor knowledge of the actual prehistory is available for both the convection and precipitation. For the empirically driven TDIM simulation (Plate 5b) the major difference is the presence of high densities in orbits 6 and 7 that occur across the polar cap. Such a density ridge is not observed at this time although it is found a few orbits later. This ridge is due to the Heppner and Maynard convection pattern that is producing a well-defined SED type feature that lines up with the satellite trajectory. This feature can be seen in Plate 2, lower set of panels labeled 1, 2, and 3.

At the onset of the storm when satellite orbits 8, 9, and 10 are just skimming the cusp-dayside oval, the TDIM shows highly depleted densities everywhere. However, the observations show a dusk region of enhanced densities, which are probably associated with the SED region that *Foster* [1993] finds that extends from the cusp to lower midlatitudes in the afternoon sector as a storm begins. Neither TDIM simulation has captured such a SED event.

From orbit 11 through 14 the storm has developed. The polar region is observed to be depleted with densities on both the dawn and dusk side dropping well below 10^4 cm^{-3}. In the center of the polar region, or just to the duskside, a TOI density enhancement is observed with densities exceeding 10^5 cm^{-3}. These observations are well reproduced by the MHD-TDIM simulation. This agreement continues over three orbits, or 4 hours, and occurs during a major storm. The *Dst* is below -100γ, and the *Kp* is above 6. There is no equivalent agreement between the empirically driven TDIM simulations and observations.

7. Discussion

The magnetic cloud passage event of January 14, 1988, is ideal for demonstrating ionospheric response to magnetospheric forcing in several different ways. First, the IMF rate of change is relatively slow with a time constant of the order of 1/2 to 1 hour. This time constant is almost the same as that of the *F* region. Hence the case can be made that the changing magnetosphere could be approximated by a series of steady states, i.e., empirical patterns. This is in fact the argument used to justify one of the two TDIM simulations. Second, the magnetic cloud passage has a northward IMF period followed by a southward period; the complex, but substorm free, northward period is not contaminated by long-term ionospheric-thermospheric changes that result from southward IMF storm periods. Hence the ionosphere's response to strong northward conditions lasting more than 10 hours can be studied relatively straightforwardly. A third reason why this is an ideal event lies in the extensive monitoring of the solar wind, magnetosphere, and ionosphere. This has led to a series of research papers that have interpreted the magnetospheric response to the event [*Cumnock et al.*, 1992; *Freeman et al.*, 1993; *Knipp et al.*, 1993, 1994]. In turn, this has set the stage for this study which uses the NRL-MHD model magnetospheric electric field and auroral precipitation patterns [*Slinker et al.*, 1995] as drivers for one of the TDIM simulations. This provides a unique first simulation of the ionosphere's response to self consistent electric field and auroral precipitation patterns over a 24-hour period that leads into a major geomagnetic storm. Given the favorable attributes of this event, an expectation exists to have good confidence in the MHD representation of the magnetosphere's morphology, the subsequent imposition of these electric fields and auroral precipitation into the ionosphere, and hence that the ionospheric simulation is well constrained in the dominant weather inputs for this event.

The TDIM simulations contrasting the MHD and empirical inputs are significantly different. The differences are on both a large morphological scale as well as fine structure differences such as the TOI. In comparing these simulations the dominant *F* region input is the electric field, both in frictional heating effects as well as transport effects. In section 5 the comparisons emphasized the role of the electric field, while the auroral precipitation patterns was secondary in the *F* region. This would not be the case in the *E* region where the roles would almost be reversed. From a climatology point of view this study has been carried out in the summer hemisphere which is usually viewed as being relatively smooth and not sensitive to weather, though this study clearly shows that even in sunlight significant weather features are imposed in the *F* region ionosphere. A polar hole is created in both the empirical and MHD simulation; the depths are clearly different with the MHD case being at least twice as deep. Even during the northward period, which would usually be viewed as relatively quiet, the MHD model develops many weather features that are based on highly depressed *F* region densities. In this case the MHD reverse convection cells achieve 80 kV, a cross-tail potential magnitude normally associated with disturbed ionospheric features. These include the new reverse flow TOI feature.

Overall confidence in the TDIMs marked summer ionosphere response to the MHD magnetospheric drivers is given by the comparisons with the DMSP-F8 electron density observations at 840 km. Both weather features and large-scale morphology agree well. The period of disagreement at the storm beginning, F8 orbits 8, 9, and 10, also occurs when the satellite is skimming the dayside auroral oval. This discrepancy is an indication either that the simulated electric fields in both the MHD and empirical cases have not expanded equatorward enough to reach the satellite or that neither electric field is able to generate the needed conditions to produce the SED feature [*Foster*, 1993]. This feature needs further follow up since it hinges upon how well the electric field model is able to penetrate to lower latitudes, including how it is shielded by the ring currents, the physics of which is missing from the MHD model and is not represented in the empirical model.

Although during the event the empirically driven simulation does not agree with the MHD simulation it is only during the storm period that it appears to be unable to generate the observed features. This is an oversimplification; the empirically driven simulation results do show polar holes and tongues of ionization it is just that the magnitude, positioning, or orientation are not correct. Further work needs to be carried out to see if more sophisticated empirical models produce improved agreement (e.g., the more recent *Weimer* [1995] empirical convection model).

This study has achieved a milestone in that self consistent electric field and electron precipitation imposed upon the ionosphere have driven an ionospheric model to produce a weather morphology that does agree with ionospheric observations. Although not all encompassing this magnetosphere-ionosphere study has demonstrated that significant differences exist between climatological drivers and MHD drivers, even when the solar wind rate of change is

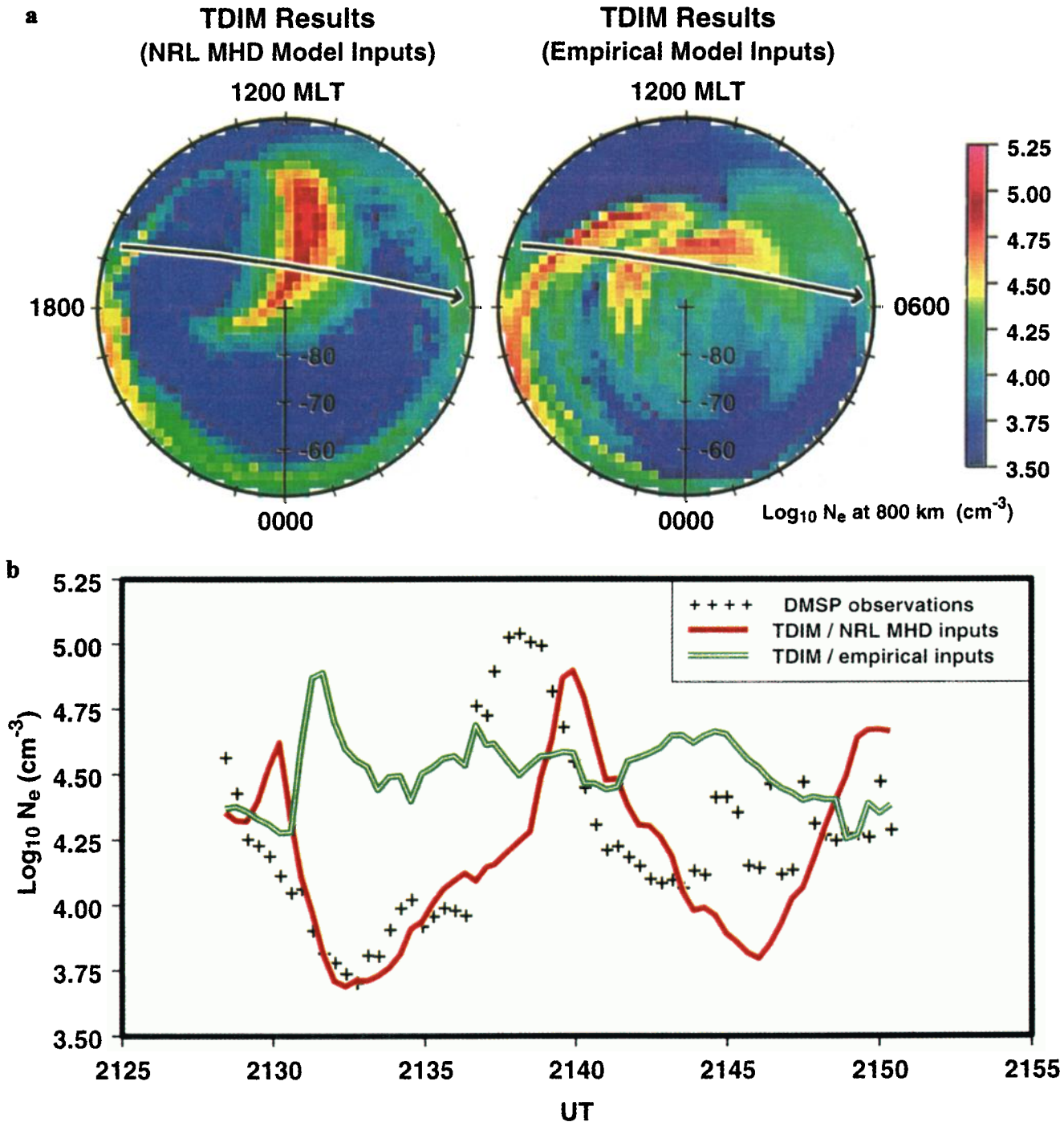

Plate 4. DMSP-F8 electron density comparison with two TDIM simulations (Plate 4b) for orbit 13. Plate 4a shows snapshots of the electron density at 800 km from the two TDIM simulations with the orbit 13 path superimposed.

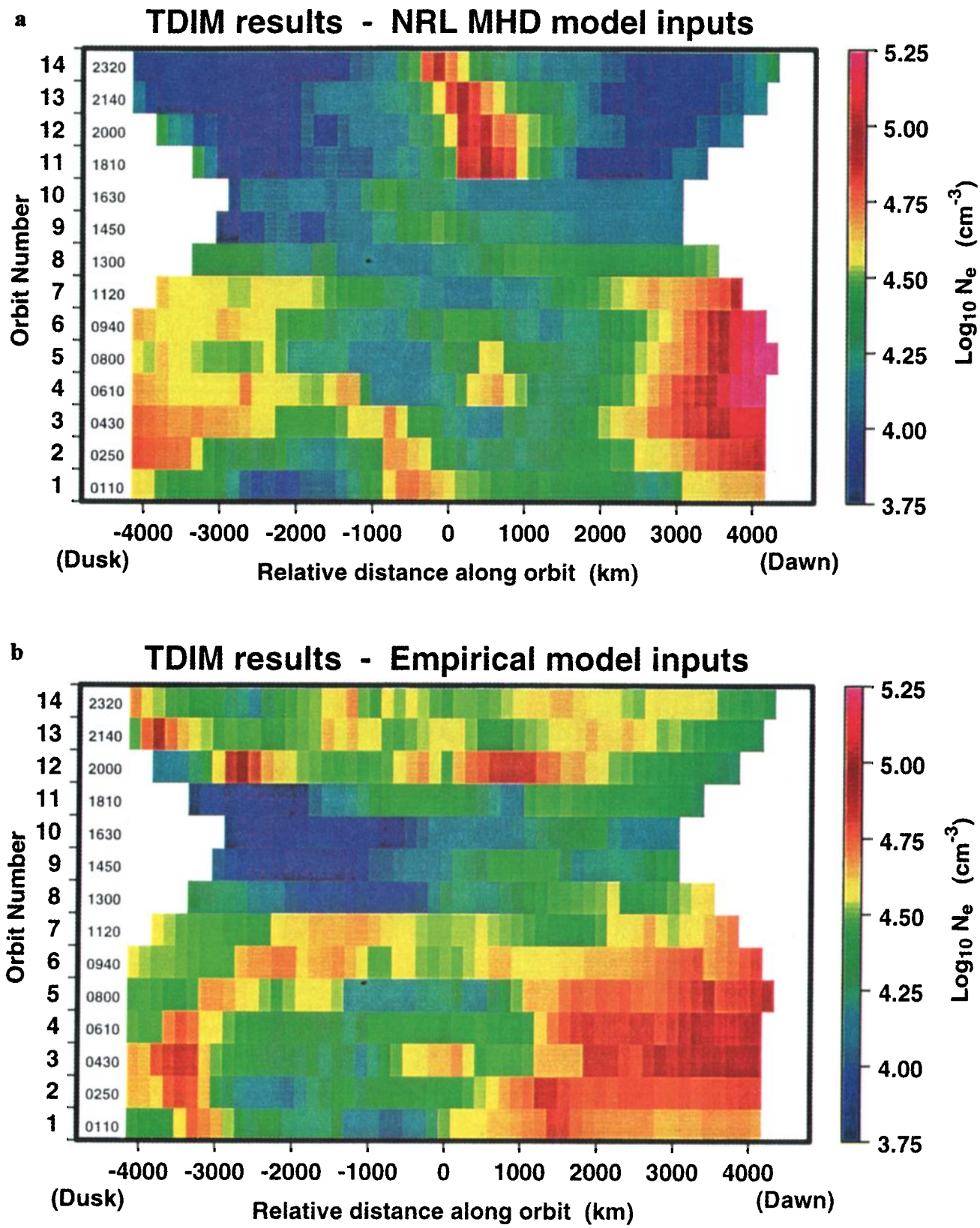

Plate 5. Summary of electron density for two TDIM simulations plotted in a format to be compared with the DMSP-F8 electron density observations shown in Plate 1.

slow enough to indicate that climatological drivers might be adequate.

8. Conclusion

This study has successfully simulated the ionospheric response to the passage of a magnetic cloud past the Earth. The key findings of this study are the following:

1. The January 14, 1988, event created well defined ionospheric features that were observed in the topside ionosphere by the DMSP-F8 satellite. These observations were used to distinguish between two TDIM ionospheric simulations.

2. Agreement with observations was found in the TDIM simulation that used magnetospheric electric field and auroral precipitation inputs generated by the NRL MHD magnetospheric model.

3. Agreement was not found with the empirical input TDIM simulation.

4. The observations and MHD-TDIM simulation show several noteworthy features; (1) A large density depletion is created at the center of the summer polar ionosphere during the strongly northward IMF period and even more markedly during the southward IMF storm period. (2) A high-density TOI develops near the cusp extending into the polar cap. (3) Over an order of magnitude density change in the sunlit summer ionosphere is caused by the event. Such density gradients would probably be on a scale size adequate to cause the growth of the gradient drift instability which in turn would feed smaller-scale irregularities and hence cause space weather effects such as RF scintillations and backscatter clutter.

5. During the northward IMF period the MHD TDIM simulation generated a new feature, namely a reverse flow TOI.

This study demonstrates the potential of magnetospheric MHD modeling to generate electric field and electron precipitation patterns that can reasonably drive an ionospheric model. Noted in this study was the fact that the SED event was not successfully modeled. This feature probably depends on the storm electric fields expanding equatorwards and interfacing with the ring current system. These physical processes are not included in the present-day MHD models; further work needs to be carried out in the ionosphere to assess the magnitude and significance of the SED effect as well as reviewing the MHD formulations to determine how such non-MHD processes might be accounted for in the model.

A summer study was undertaken mainly because the magnetospheric convection patterns in the southern summer hemisphere were relatively simple 1, 2, 3, or 4 cell. In the northern hemisphere, which was under winter conditions, the convection patterns under northward IMF conditions were very complex and indeed not resolved. Further work is needed in comparing the summer and winter ionospheric responses as well as attempting to resolve the convection patterns or at least assess the degree of spatial and temporal fluctuation that exists.

This study is for a rather ideal, well-documented, magnetic cloud passage event. Other such events are being monitored and under the label of coronal mass ejection (CME) events a large body of solar wind-magnetosphere data is being collected. Hence the follow-on research needs to determine if the good agreement between this MHD-TDIM simulation and ionospheric observations will stand the test of repetition.

Acknowledgments. This research was supported by NASA grant NAG5-1484 and NSF grant ATM-9612638 to Utah State University. The work at the Naval Research Laboratory was supported by the office of Naval Research. The work at George Mason University is supported by NSF grant ATM 9613815. F. Rich is thanked for his assistance with the DMSP SSIES data.

The Editor thanks Marc Hairston and Christophe Peymirat for their assistance in evaluating this paper.

References

Bowline, M. D., J. J. Sojka, and R. W. Schunk, Ionospheric simulation driven by magnetospheric MHD inputs: Comparison with empirical input simulations and observations (abstract), *Eos Trans. AGU, 77*(46), Fall Meet. Suppl., F527, 1996.

Chen, J., S. Slinker, J. A. Fedder, and J. G. Lyon, Simulation of geomagnetic storms during the passage of magnetic clouds, *Geophys. Res. Lett., 22*, 1749-1752, 1995.

Coroniti, F. V., and C. F. Kennel, Can the ionosphere regulate magnetospheric convection?, *J. Geophys. Res., 78*, 2837-2851, 1973.

Cumnock, J. A., R. A. Heelis, and M. R. Hairston, Response of the ionospheric convection pattern to a rotation of the interplanetary magnetic field on January 14, 1988, *J. Geophys. Res., 97*, 19449-19460, 1992.

Farrugia, C. J., M. P. Freeman, L. F. Burlaga, R. P. Lepping, and K. Takahishi, The Earth's magnetosphere under continued forcing: Substorm activity during the passage of an interplanetary magnetic cloud, *J. Geophys. Res., 98*, 7657-7671, 1993.

Fedder, J. A., and J. G. Lyon, The solar wind-magnetosphere-ionosphere current-voltage relationship, *Geophys. Res. Lett., 14*, 880-883, 1987.

Fedder, J. A., and J. G. Lyon, The Earth's magnetosphere is 165 R_E long: Self-consistent currents, convection, magnetospheric structure, and processes for northward interplanetary magnetic field, *J. Geophys. Res., 100*, 3623-3635, 1995.

Fedder, J. A., J. G. Lyon, S. P. Slinker, and C. M. Mobarry, Topological structure of the magnetotail as a function of interplanetary magnetic field direction, *J. Geophys. Res., 100*, 3613-3621, 1995a.

Fedder, J. A., S. P. Slinker, J. G. Lyon, and R. D. Elphinstone, Global numerical simulation of the growth phase and the expansion onset for a substorm observed by Viking, *J. Geophys. Res., 100*, 19,083-19,093, 1995b.

Foster, J. C., Storm time plasma transport at middle and high latitudes, *J. Geophys. Res., 98*, 1675-1689, 1993.

Freeman, M. P., C. J. Farrugia, L. F. Burlaga, M. R. Hairston, M. E. Greenspan, J. M. Ruohoniemi, and R. P. Lepping, The interaction of a magnetic cloud with the Earth: Ionospheric convection in the northern and southern hemispheres for a wide range of quasi-steady interplanetary magnetic field conditions, *J. Geophys. Res., 98*, 7633-7655, 1993.

Hardy, D. A., M. S. Gussenhoven, R. Raistrick, and W. J. McNeil, Statistical and functional representations of the pattern of auroral energy flux, number flux, and conductivity, *J. Geophys. Res., 92*, 12,275-12,294, 1987.

Hedin, A. E., MSIS-86 thermospheric model, *J. Geophys. Res., 92*, 4649-4662, 1987.

Hedin, A. E., et al., Revised global model of thermospheric winds using satellite and ground-based observations, *J. Geophys. Res., 96*, 7657-7688, 1991.

Heppner, J. P., and N. C. Maynard, Empirical high-latitude electric field models, *J. Geophys. Res., 92*, 4467-4489, 1987.

Knipp, D. J., et al., Ionospheric convection response to slow, strong variations in a northward interplanetary magnetic field: A case study for January 14, 1988, *J. Geophys. Res., 98*, 19273-19292, 1993.

Knipp, D. J., B. A. Emery, A. D. Richmond, and M. R. Hairston, Mapping ionospheric convection response to IMF B_y negative and B_z positive conditions, *J. Atmos. Terr. Phys., 56*, 223-235, 1994.

Rich, F. J., and M. Hairston, Large-scale convection patterns observed by DMSP, *J. Geophys. Res., 99*, 3827-3844, 1994.

Schunk, R. W., A mathematical model of the middle and high latitude ionosphere, *Pure Appl. Geophys., 127*, 255-303, 1988.

Schunk, R. W., and J. J. Sojka, Ion temperature variations in the daytime high-latitude *F* region, *J. Geophys. Res., 87*, 5169-5183, 1982.

Schunk, R. W., and J. C. G. Walker, Theoretical ion densities in the lower ionosphere, *Planet. Space Sci., 21*, 1875-1896, 1973.

Schunk, R. W., W. J. Raitt, and P. M. Banks, Effect of electric fields on the daytime high-latitude *E* and *F* regions, *J. Geophys. Res., 80*, 3121-3130, 1975.

Schunk, R. W., P. M. Banks, and W. J. Raitt, Effect of electric fields and other processes upon the nighttime high-latitude *F* layer, *J. Geophys. Res., 81*, 3271-3282, 1976.

Schunk, R. W., J. J. Sojka, and M. D. Bowline, Theoretical study of the electron temperature in the high-latitude ionosphere for solar maximum and winter conditions, *J. Geophys. Res., 91*, 12,041-12,054, 1986.

Slinker, S. P., J. A. Fedder, J. Chen, and J. G. Lyon, Deducing global magnetosphere indices and ionospheric energy input for the storm of January 14, 1988 from an MHD simulation (abstract), *Eos Trans. AGU, 76*, Fall Meeting Suppl., F499, 1995.

Sojka, J. J., Global scale, physical models of the *F* region ionosphere, *Rev. Geophys., 27*, 371-403, 1989.

Sojka, J. J., W. J. Raitt, and R. W. Schunk, A theoretical study of the high-latitude winter *F* region at solar minimum for low magnetic activity, *J. Geophys. Res., 86*, 609-621, 1981a.

Sojka, J. J., W. J. Raitt, and R. W. Schunk, Theoretical predictions for ion composition in the high-latitude winter *F* region for solar minimum and low magnetic activity, *J. Geophys. Res., 86*, 2206-2216, 1981b.

Sojka, J. J., R. W. Schunk, M. D. Bowline, J. Chen, S. Slinker, and J. Fedder, Driving a physical ionospheric model with a magnetospheric MHD model, *J. Geophys. Res., 102*, 22,209-22,220, 1997.

Weimer, D. R., Models of high-latitude electric potentials derived with a least error fit of spherical harmonic coefficients, *J. Geophys. Res., 100*, 19,595-19,607, 1995.

M. D. Bowline, R. W. Schunk, and J. J. Sojka, Center for Atmospheric and Space Sciences, Utah State University, Logan, UT 84322-4405. (e-mail: fasojka@sojka.cass.usu.edu; schunk@cc.usu.edu; usera@theor3.cass.usu.edu)

J. Chen and S. Slinker, Plasma Physics Division, Naval Research Laboratory, Washington, DC 20375. (e-mail: chen@ppdu.nrl.navy.mil; slinker@ppdu.nrl.navy.mil)

J. Fedder, Institute for Computational Sciences and Informatics, George Mason University, Fairfax, VA 22030-4444. (e-mail: fedder@ppdu.nrl.navy.mil)

P. J. Sultan, Air Force Research Laboratory, Space Effects Division/GPSM, 29 Randolph Road, Hanscom AFB, MA 01731. (e-mail: sultan@plh.af.mil)

(Received February 23, 1998; revised April 13, 1998;
accepted May 13, 1998)